International Journal of Modern Physics B
Vol. 29, No. 6 (2015) 1550036 (13 pages)

DOI: 10.1142/S0217979215500368

World Scientific
www.worldscientific.com

Approximating metal–insulator transitions

Carlo Danieli*,‡, Kristian Rayanov*, Boris Pavlov†, Gaven Martin† and Sergej Flach*

*New Zealand Institute for Advanced Study,
Centre for Theoretical Chemistry and Physics, Massey University,
Auckland, New Zealand
†New Zealand Institute for Advanced Study, Massey University,
Auckland, New Zealand
‡c.danieli@massey.ac.nz

Received 2 September 2014
Revised 10 November 2014
Accepted 11 November 2014
Published 15 December 2014

We consider quantum wave propagation in one-dimensional quasiperiodic lattices. We propose an iterative construction of quasiperiodic potentials from sequences of potentials with increasing spatial period. At each finite iteration step, the eigenstates reflect the properties of the limiting quasiperiodic potential properties up to a controlled maximum system size. We then observe approximate Metal–Insulator Transitions (MIT) at the finite iteration steps. We also report evidence on mobility edges, which are at variance to the celebrated Aubry–André model. The dynamics near the MIT shows a critical slowing down of the ballistic group velocity in the metallic phase, similar to the divergence of the localization length in the insulating phase.

Keywords: Quasiperiodic; Aubry–André model; metal–insulator transitions.

PACS numbers: 03.75.Lm, 72.20.Ee, 72.15.Rn

1. Introduction

Wave localization in random potentials has been intensively studied ever since its prediction by Anderson in the year 1958.[1] Notably uncorrelated random potentials in space dimension $d = 1$ will lead to complete localization. Metal–Insulator Transitions (MIT) and possible mobility edges (energies separating delocalized (metallic) from localized (insulating) eigenstates) will typically appear in systems with space dimension $d = 3$. Later studies of potentials with correlated disorder have shown that the dimension restriction for an MIT can be lowered to $d = 1$ if there are sufficiently strong correlations in the disorder potential.[2]

It came as a surprise that the quasiperiodic potential introduced by Aubry and André (AA) in 1980, allowed an MIT when $d = 1$.[3] This MIT is tuned by the

strength λ of a $\cos(2\pi\alpha\ell)$ potential whose period $1/\alpha$ is irrational and therefore incommensurate with the lattice spacing $\Delta\ell = 1$. Analytical results were obtained thanks to a duality principle relating states and spectra in direct and Fourier space. This very principle prevents the appearance of mobility edges. The MIT between extended or localized states of the AA model is not dependent on the eigenenergy but only on the potential strength λ. Attempts to generalize these results to other quasiperiodic potentials for $d = 1$, showed that the localized regime could be maintained irrespective of the potential strength.[4] Further, Fibonacci sequence based potentials kept the system at the critical point[5,6] and a mix of two AA potentials with different periods, also known as the bichromatic quasiperiodic lattice, allowed the appearance of a mobility edge.[7–9] A recent study of two interacting particles in the AA model, established the appearance of metallic correlated bound states deep in the insulating regime for a single particle.[10]

Experimental studies on light propagating through optical waveguide networks[11] and ultracold atomic clouds expanding in optical potentials[12] successfully tested the MIT within the AA model. The flexibility in the choice of potentials within these studies makes them ideal testing grounds for other quasiperiodic potentials. A discussion about possible experimental observations of the mobility edge in the bichromatic lattice can be found in Ref. 8. At the same time these systems have finite size and have unavoidable precision limitations on the generated potentials.[13] Desired effects like the MIT or mobility edges are therefore needed only up to that precision, and only to be observable on these length scales, see also Ref. 9.

In this paper, we present a systematic and constructive way to approximate a quasiperiodic potential by a periodic one. Each approximation is defined both by its period and by the convergence criteria of the amplitude sequence of higher harmonics. This flexibility allows us to obtain a wide variety of quasiperiodic potentials which can be expected to exhibit the above phenomena. In addition, the experimentally relevant length scale can be easily taken into account by the corresponding periodic approximation of a quasiperiodic potential.

The paper is structured as follows: in Sec. 2, we briefly discuss the AA model and some lesser-known properties of wave packet spreading. Section 3 introduces the construction principle for the new class of quasiperiodic potentials. Section 4 discusses the main properties of localized and extended states for particular amplitude sequences. Finally we conclude and summarize.

2. Aubry–André Model

Consider the $d = 1$ dimensional discrete Schrödinger operator $H : \ell^2(\mathbb{Z}) \to \ell^2(\mathbb{Z})$, also known as AA model, defined by

$$(H\psi)_l = \epsilon_l\psi_l + \psi_{l+1} + \psi_{l-1}\,, \quad l \in \mathbb{Z}\,, \tag{1}$$

with quasiperiodic potential

$$\epsilon_l = \lambda\cos(2\pi(\alpha l + \beta))\,, \quad \alpha \in \mathbb{R}\setminus\mathbb{Q}\,, \tag{2}$$

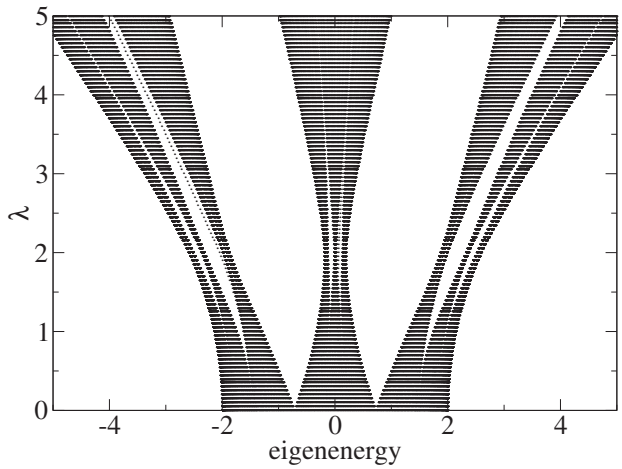

Fig. 1. Spectrum σ_λ of the AA model when $\alpha = (\sqrt{5}-1)/2$.

with a positive real strength $\lambda > 0$, $\beta \in \mathbb{R}$ and irrational α.[a] Due to the self-dual character at $\lambda = 2$, the model exhibits a transition between a metallic phase for $\lambda \in]0, 2[$ and an insulating phase when $\lambda \in]2, +\infty[$. It is also well-known as for Ref. 3 that, for any given λ in the insulating phase, all normal modes decay exponentially in space as $e^{-l/\xi}$, with the localization length $\xi = 1/\ln(\lambda/2)$ being independent of the eigenenergy.

The eigenenergy spectrum $\sigma_\lambda(\alpha, \beta)$ of the AA model has a Cantor set structure for all $\lambda \neq 0$.[14] When the incommensurate parameter is chosen as the golden mean $\alpha = (\sqrt{5}-1)/2$, the spectrum exhibits a self-similar structure, which consists of three bands, each of which again consists of three sub-bands and so forth (Fig. 1). The self-similar structure does not depend on β. The Lebesgue measure[15] can be found analytically by the formula

$$\mu(\sigma_\lambda) = 2|2 - |\lambda|| \,.$$

For $\lambda \in]0, 2[$ (metallic phase), the model has absolutely continuous spectrum,[16] while for $\lambda \in]2, +\infty[$ (insulating phase) it is a purely point spectrum.[17] At the critical value $\lambda = 2$, the spectrum is purely singular continuous.[18] The spectrum's fractal dimension has been the object of several studies, in particular at the critical value. For $\lambda \neq 2$ in 1986 Tang *et al.*[19] showed that the fractal measure is 1. Instead, at the critical value $\lambda = 2$, former studies[19–21] show that the fractal dimension is 0.5. Note that our working golden mean value for α is covered by the above statements. Latter works[22,23] show that 0.5 is in fact an upper bound, and find classes of irrational numbers α for which the correspondent spectrum's fractal dimension is lower than 0.5.

[a]We explicitly exclude rational values of α from our considerations.

Remarkably, there are much more exact results for the spectral properties of the AA model, as compared to the dynamical properties of wave packet spreading

$$i\dot{\psi}_l = (H\psi)_l \,, \tag{3}$$

where the numerical results are known.[13,23,24]

Consider a single site excitation for a normalized wave function $\sum_l |\psi_l|^2 = 1$. Its evolution in time leads to a time-dependent distribution $n_l(t) = |\psi_l(t)|^2$. The dynamics can be characterized by the second moment $m_2 = \sum_l (l - \sum_k k n_k)^2 n_l$, which in a delocalized regime is expected to grow algebraically in time $m_2 \sim t^\gamma$ with real exponent γ. For the case of the golden mean, we can distinguish three different notable spreading regimes[13,24]:

$$m_2 \sim \begin{cases} v_g^2 t^2 & \text{Ballistic Spreading}\,, \\ Dt & \text{Diffusive Spreading}\,, \\ \xi^2 & \text{Localization}\,, \end{cases}$$

where the coefficients are: the group velocity v_g, the diffusion coefficient D and the localization length ξ. In particular, spreading is expected to be ballistic in the metallic regime $\lambda < 2$ and diffusive at the critical point $\lambda = 2$.[13,24] Other studies[23] showed cases where at the critical value the spreading is slightly subdiffusive (with $\gamma \lesssim 1$). Further interesting issues concerning the connection between the spectral measure, the fractal dimension, temporal correlations and the diffusive growth.[25] We plot our calculations of the time evolution of the second moment for the different regimes in Fig. 2.

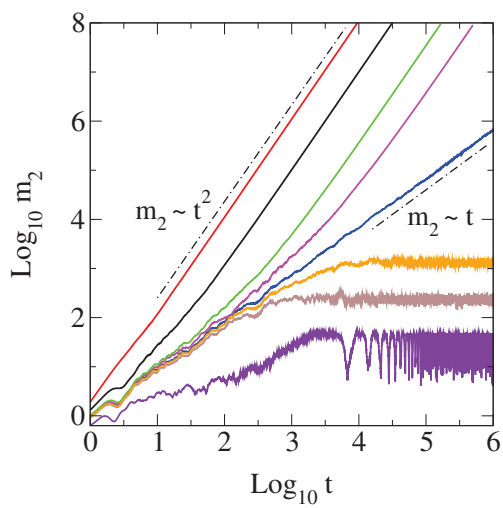

Fig. 2. (Color online) The second moment m_2 for a single site excitation as a function of time in a log–log plot. From top to bottom: $\lambda = 0.5$ (red), $\lambda = 1.5$ (black), $\lambda = 1.9$ (green), $\lambda = 1.97$ (orange), $\lambda = 2$ (blue), $\lambda = 2.05$ (brown) and $\lambda = 2.5$ (violet). The dashed-dotted lines indicate power laws $m_2 \sim t$ (diffusive) and $m_s \sim t^2$ (ballistic). Here $\alpha = (\sqrt{5} - 1)/2$ and $\beta = 0$.

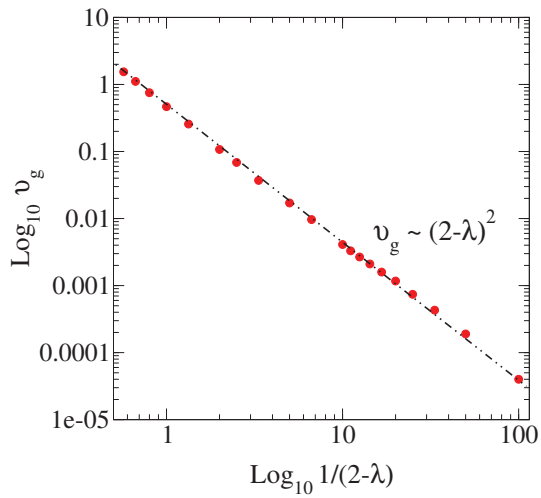

Fig. 3. (Color online) The dependence of the group velocity v_g on $1/(2-\lambda)$ in the metallic phase in a log–log plot. The symbols are the actual computed values, the dashed line corresponds to the law $v_g \sim (2-\lambda)^2$.

We see that for $\lambda = 2$ spreading appears to be diffusive..[13,24] However we can not exclude a slightly subdiffusive spreading with $\gamma \approx 0.95$ as reported in Ref. 23. We also confirm the predicted ballistic asymptotics in the metallic regime and localization in the insulating regime. However, we also observe a diffusive transient in these regimes, which becomes longer, the closer one gets to the critical point. We compute the group velocity v_g, which is given by the square root of m_2 up to a constant prefactor, and plot it in Fig. 3. We find that it vanishes at the critical point as $v_g \sim (2-\lambda)^2$.

It remains an intriguing task to explain these spreading regimes in their relation to the Cantor spectrum of the model. This concerns in particular, the crossover time τ_λ, the critical exponent for v_g and the question why spreading into a large but finite localization volume in the insulating regime happens to be diffusive and not ballistic, as for one-dimensional uncorrelated disorder (Ref. 26). These observations may be rather special features of the highly symmetric AA model which enjoys duality.

3. Cantor-Like Constructions of a Class of Quasiperiodic Potentials

We now construct quasiperiodic potentials in a systematic way, approximating them by periodic potentials at each iteration step. The standard construction of a 1/3 Cantor set (cut out the middle third of an interval, then repeat with the remaining subintervals *ad infinitum*) gives a set of measure zero and nonzero Hausdorff dimension $\log 2/\log 3$. Here we modify this procedure for the eigenenergy spectrum effectively, by stretching and changing the cutting ratio. This is all achieved by

defining sequences of periodic potentials with increasing spatial period. For simplicity, we shall start with an example which has a three band structure (where each band, again subdivides into three sub-bands etc.) similar to the golden mean case of the AA spectrum before we generalize.

3.1. *The scheme*

Consider a sequence of discrete periodic functions $E_k(l)$ with $k = 1, 2, 3, \ldots$. Each function is periodic with spatial period $L_k = 3^k$: $E_k(l + L_k) = E_k(l)$. The function E_1 has period $L_1 = 3$ and is defined for $l \in \mathbb{Z}$ and for a real positive value a_1 by

$$E_1(l) = \begin{cases} -a_1 & l = 3m\,, \\ 0 & l = 3m + 1\,, \\ +a_1 & l = 3m + 2\,. \end{cases} \quad m \in \mathbb{Z}\,,$$

and it has the schematic form represented in Fig. 4.

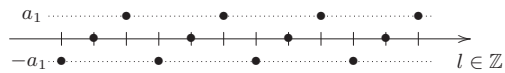

Fig. 4. Schematic picture of the potential E_1 for a real positive value a_1.

The second function E_2 has period $L_2 = 9$ and is defined for $l \in \mathbb{Z}$ and for a real positive value a_2 by

$$E_2(l) = \begin{cases} -a_2 & l = 9m + \{0, 1, 2\}\,, \\ 0 & l = 9m + \{3, 4, 5\}\,, \\ +a_2 & l = 9m + \{6, 7, 8\}\,. \end{cases} \quad m \in \mathbb{Z}\,,$$

and it has the schematic form represented in Fig. 5.

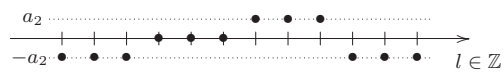

Fig. 5. Schematic picture of the potential E_2 for a real positive value a_2.

Higher order functions $E_k(l)$ are defined in a similar way for $l \in \mathbb{Z}$ and are characterized by the corresponding real positive amplitude a_k:

$$E_k(l) = \begin{cases} -a_k & \text{if } l = 3^k m + q\,, \\ 0 & \text{if } l = 3^{k-1}(3m + 1) + q\,, \\ +a_k & \text{if } l = 3^{k-1}(3m + 2) + q\,, \end{cases} \quad m \in \mathbb{Z}\,,$$

with $0 \leq q \leq 3^{k-1} - 1$, and their schematic form is represented in Fig. 6.

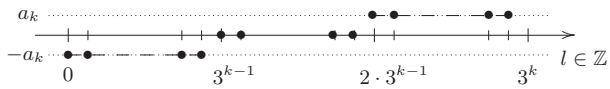

Fig. 6. Schematic picture of the potential E_k for a real positive value a_k.

Now we consider the superposition of all $E_k(l)$ for all $1 \leq k \leq K$:

$$\epsilon_{l,K} = \lambda \sum_{k=1}^{K} E_k(l)\,, \quad \forall\, l \in \mathbb{Z}\,, \tag{4}$$

where $\lambda > 0$ is again the potential strength parameter. The potential $\epsilon_{l,K}$ is periodic with period L_K. For example, for $K = 2$ we obtain a potential of period $L_2 = 9$: $\epsilon_{l,2} = E_1(l) + E_2(l)$ with the spatial profile represented in Fig. 7.

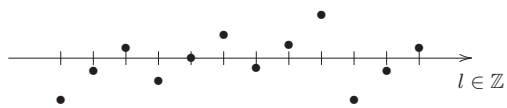

Fig. 7. Schematic picture of the potential $E_1 + E_2$ for the real positive value a_1 and a_2.

The same construction could be done for sequences of periodic functions $E_{k,s}(l)$ with $k = 1, 2, 3, \ldots$ of spatial period $L_{k,s} = s^k$ with $s \in \mathbb{N}$: $E_{k,s}(l + L_{k,s}) = E_{k,s}(l)$. We can simplify notations by using the definition $[l]_m \equiv l \bmod m$ to arrive at

$$E_{k,s}(l) = \left(\left\lfloor \frac{[l]_{s^k}}{s^{k-1}} \right\rfloor - \left\lfloor \frac{s}{2} \right\rfloor \right) a_k =: \phi_{k,s}(l) a_k\,, \quad \forall\, l \in \mathbb{Z}\,,$$

defined for a_k a real positive number. The bracket $\lfloor \cdot \rfloor$ denotes the integer part of a real number. The final expression for the potential $\epsilon_{l,K}$ defined in Eq. (4) is

$$\epsilon_{k,K} := \lambda \sum_{k=1}^{K} \phi_{k,s}(l) a_k\,, \quad \forall\, l \in \mathbb{Z}\,, \tag{5}$$

where $\{a_k\}_{k=1}^K$ is the generating sequence of the potential and $\{\phi_{k,s}(l)\}_{k=1}^K$ the partitioning sequence.

In the absence of any potential ϵ_l, the spectrum of the operator [Eq. (1)] is given by one band $\sigma = 2\cos p$ where p is a Bloch wave number. For $K = 1$ and in the case $s = 3$, the spectrum splits into three bands which are separated by two gaps. The first step in the above construction therefore, cuts two segments out of the one band spectrum. At the next step of the approximation $K = 2$, the spatial period $L_2 = 9$ and the spectrum consists now of 9 bands and 8 gaps. Therefore, each of the three bands of the $K = 1$ spectrum is split into three narrower ones, with the new subgaps, removing parts of the $K = 1$ bands. At the same time, the bands edges may also shift, thus we obtain a Cantor-like iterative construction.

3.2. *The quasiperiodic limit*

We now push the iterative construction to its limit by extending Eq. (5) to an infinite sum

$$\epsilon_l = \lambda \sum_{k=1}^{+\infty} \phi_{k,s}(l) a_k \,, l \in \mathbb{Z} \,. \tag{6}$$

The finiteness of this sum depends on the convergence properties of the generating sequence. We make the following definition: a sequence $\{\epsilon_l\}_{l\in\mathbb{Z}}$ is *quasiperiodic* if for every $\delta > 0$, there is $T = T(\delta) > 0$ such that for all $l \in \mathbb{Z}$ we have $|\epsilon_{l+T} - \epsilon_l| < \delta$. We have the following.

Lemma 1. *Let's consider a family $\{\{\epsilon_l^k\}_{l\in\mathbb{Z}}\}_{k=0}^{+\infty}$ of potentials and suppose that for each k the sequence $\{\epsilon_l^k\}_{l\in\mathbb{Z}}$ is periodic with period L_k and the tails satisfy*

$$\lim_{N\to\infty} \sup_{l\in\mathbb{Z}} \sum_{k=N}^{\infty} \epsilon_l^k = 0 \,.$$

Then the sequence $\{\tilde{\epsilon}_l\}_{l\in\mathbb{Z}}$ defined by the sum

$$\tilde{\epsilon}_l = \sum_{k=0}^{\infty} \epsilon_l^k \,, \tag{7}$$

is quasiperiodic.

The proof is simply to observe that any partial sum $\sum_{k=0}^{N} \epsilon_l^k$ is periodic with period $T_N = lcm(L_1, L_2, \ldots, L_N)$ (here lcm means least common multiple) and that the tail sums $\sum_{k=N}^{\infty} \epsilon_l^k$ are uniformly small, independent of l. So, for a given $\delta > 0$, we choose $N = N(\delta)$ such that

$$\sup_{l\in\mathbb{Z}} \sum_{k=N+1}^{\infty} \epsilon_l^k < \frac{\delta}{2} \,.$$

It follows that $\forall\, l \in \mathbb{Z}$ we have

$$\begin{aligned} |\tilde{\epsilon}_{l+T_N} - \tilde{\epsilon}_l| = \Bigg| & \sum_{k=0}^{N} \epsilon_{l+T_N}^k + \sum_{k=N+1}^{+\infty} \epsilon_{l+T_N}^k \\ & - \sum_{k=0}^{N} \epsilon_l^k - \sum_{k=N+1}^{+\infty} \epsilon_l^k \Bigg| < 2 \cdot \frac{\delta}{2} = \delta \,. \end{aligned}$$

The property of quasiperiodicity stated above holds for the potential $\tilde{\epsilon}_l$ stated in Eq. (7). This ends the proof of the lemma.

As a direct corollary, we see that the potential defined by Eq. (6) is quasiperiodic. Thus the above class of potentials, which is defined by its generating sequence $\{a_k\}_{k=1}^{+\infty}$ and the choice of the integer s of the partitioning sequence $\{\phi_{k,s}(l)\}_{k=1}^{+\infty}$, is quasiperiodic.

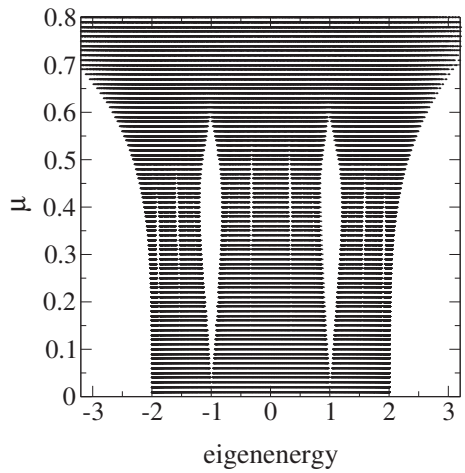

Fig. 8. Model A. The eigenenergy spectrum versus μ. Here $s = 3$, $\lambda = 1$ and $K = 9$.

4. Numerical Results

In this section, we first analyze a particular case A of potentials, defined by the geometric sequence $a_k = \mu^k$ (Model A), for a real value $\mu \in]0, 1[$ and $s = 3$

$$\epsilon_{l,K} = \lambda \sum_{k=1}^{K} \phi_{k,3}(l)\mu^k\,, \quad \forall\, l \in \mathbb{Z}\,. \tag{8}$$

First we consider $\lambda = 1$.

In Fig. 8, we show how the spectrum changes for different potential strength parameter $\mu \in]0, 1[$. For μ values from 0 to 0.5, the width of the spectrum and its sub-band shrinks and then, for $\mu \geq 0.5$ it starts to stretch. A similar effect is seen in the AA model spectrum around the transition value $\lambda = 2$.

To characterize localization of the corresponding eigenstates, we compute the participation number $P = 1/\sum_l |\psi_l|^4$ of each eigenmode $(\psi_l)_{l\in\mathbb{Z}}$ and consider the maximum $P_{\max}$ for a given μ.

We find that $P_{\max}^{-1}$ drops down to zero around $\mu = 0.5$, irrespective of the used system size (Fig. 9). These graphs suggest that at $\mu \leq 1/2$, some eigenstates become extended and therefore the insulating regime is lost. Calculations for other $\lambda > 0$ show how this threshold value of the loss of the insulating regime evolves continuously along the set of parameters $(\mu, \lambda) \in]0, 1\,[\times]0, +\infty[$. The outcome is shown in Fig. 10, where the MIT curve limits the red shaded area in which the metallic delocalized states appear.

A similar MIT arises for model B with the potential [Eq. 6)] using an algebraic generating sequence $a_k = 1/k^\nu$:

$$\epsilon_{l,K} = \lambda \sum_{k=1}^{K} \phi_{k,3}(l)\frac{1}{k^\nu}\,, \quad \forall\, l \in \mathbb{Z}\,. \tag{9}$$

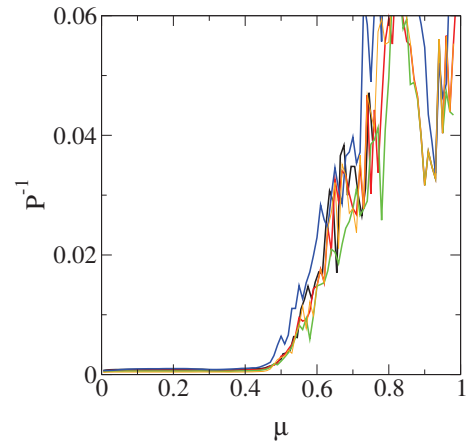

Fig. 9. (Color online) Model A. Inverse of the largest participation number $P_{\max}$ versus μ for $N = 1000, 2000, 3000, 4000, 5000$. Here $s = 3$, $\lambda = 1$ and $K = 9$.

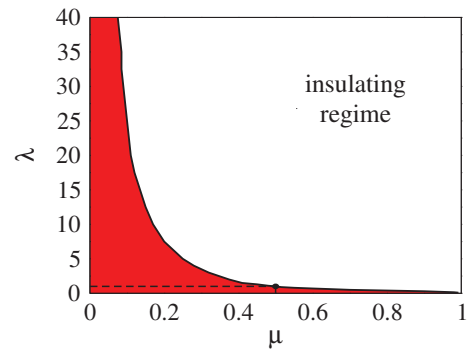

Fig. 10. (Color online) The phase diagram of model A with potential [Eq. (8)]. The red shaded area corresponds to the metallic regime (extended eigenstates exist). Here $s = 3$ and $K = 9$.

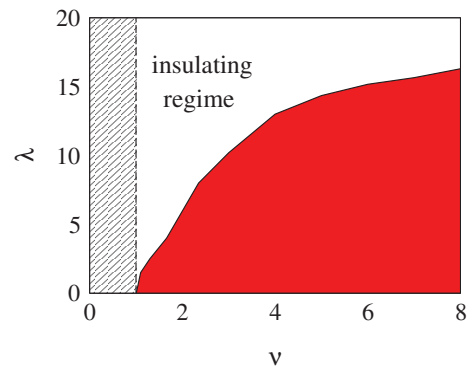

Fig. 11. (Color online) The phase diagram of model B with potential [Eq. (9)]. The red shaded area corresponds to the metallic regime (extended eigenstates exist). Here $s = 3$ and $K = 9$.

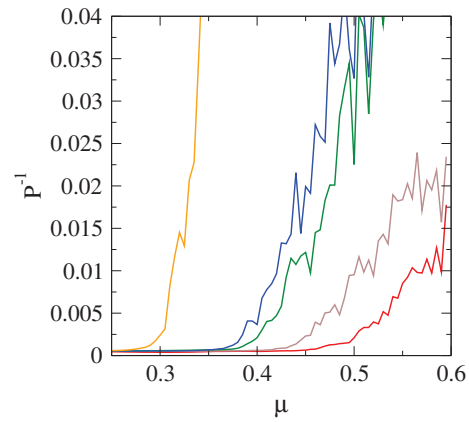

Fig. 12. (Color online) Model A. Curves of Inverse of the largest participation number $P_{\max}$ versus $\mu \in]0.25, 0.6[$ for $N = 5000$ for five evergy subintervals. From bottom to top: $0 < E < 0.31$ (red), $0.31 < E < 1$ (brown), $1 < E < 1.58$ (green), $1.58 < E < 1.92$ (blue), $1.92 < E < 2.5$ (yellow). Here $s = 3$, $\lambda = 1$ and $K = 9$.

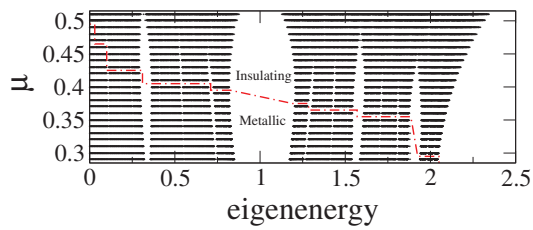

Fig. 13. (Color online) Model A. A zoom of the eigenenergy spectrum versus μ from Fig. 8. The mobility edge is indicated by the thick dashed red line. Here $s = 3$, $\lambda = 1$ and $K = 9$.

for a real value $\nu \in]1, +\infty[$. Its phase diagram is shown in Fig. 11.

Returning to model A, we compute again for $\lambda = 1$ the participation number P of eigenstates for different values $\mu \in]0.25, 0.6[$. Now we consider energy intervals which correspond to various sub-bands of the spectrum (see caption in Fig. 12). In each of these intervals we choose the largest value of $P_{\max}$ and plot its inverse as a function of μ in Fig. 12.

We find that the MIT transition values of μ and the sharpness of the transition depend on the chosen energy sub-band. Therefore we observe energy-dependent MIT values of μ, i.e., an energy-dependent mobility edge in Fig. 13.

Next we study the dynamics for the model A (similar to the AA case). We compute the time evolution of the second moment m_2 for a single site excitation for different values μ of the generating sequence in the interval $]0, 1[$ (Fig. 14).

We find that the basic properties of the AA model are qualitatively recovered. For small values $\mu \sim 0.05 - 0.1$ the spreading is close to ballistic. An increase of μ changes the dynamics: an increasingly long transient region of slower spreading is emerging. At $\mu \approx 0.5$, the dynamics is close to diffusive, up to the largest times of

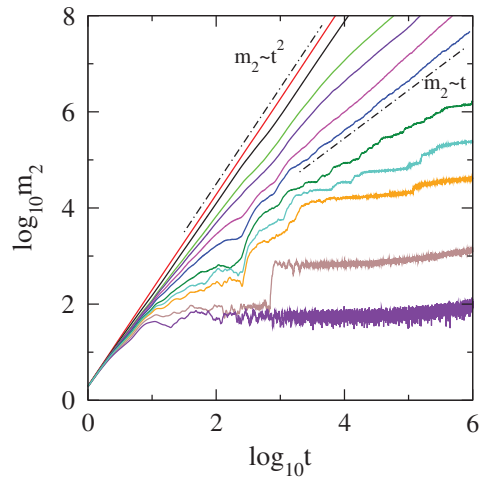

Fig. 14. (Color online) Model A. The second moment m_2 for a single site excitation as a function of time in a log–log plot. From top to bottom: $\mu = 0.05$ (red), $\mu = 0.29$ (black), $\mu = 0.4$ (green), $\mu = 0.43$ (indigo), $\mu = 0.47$ (magenta), $\mu = 0.5$ (blue), $\mu = 0.55$ (dark green), $\mu = 0.575$ (celeste), $\mu = 0.6$ (orange), $\mu = 0.65$ (brown) and $\mu = 0.7$ (purple). The dashed-dotted lines indicate power laws $m_2 \sim t$ (diffusive) and $m_2 \sim t^2$ (ballistic). Here $s = 3$, $\lambda = 1$ and $K = 9$.

computation. A more in-depth analysis of these dynamical processes can be rather interesting and complicated, especially in the parameter region of the mobility edge $0.3 \leq \mu \leq 0.5$, where extended states coexist with localized states with arbitrary large localization length. For μ closer to 1, the wave dynamics shows spreading into a finite volume, which will imply localization.

5. Summary

We obtained an iterative construction of quasiperiodic potentials from sequences of potentials with increasing spatial period. At each finite iteration step, the eigenstates reflect the properties of the limiting quasiperiodic potential properties, up to a controlled maximum system size. We observe approximate MIT at finite iteration steps. We observe mobility edges, at variance to the celebrated AA model. The dynamics near the MIT, shows a critical slowing down of the ballistic group velocity in the metallic phase. An important open question concerns the existence of suitable choices of the generating sequence, (and even different periodic modulations) so that the model has a duality principle. In particular it would be interesting to find such a special choice which will reobtain the AA case. Further, we point to the mathematical observation in Ref. 27 and its physical interpretation in Ref. 28, that few-body Hamiltonians obtained on the base of one-body Hamiltonians with singular spectrum, may have absolutely continuous branches in their spectrum. This may correlate with the numerical observation of such branches in Ref. 10. The presented potential construction algorithm may be of use for future studies in these directions.

Acknowledgments

We thank Xiaoquan Yu and Joshua Bodyfelt for useful discussions.

References

1. P. W. Anderson, *Phys. Rev.* **109**, 1492 (1958).
2. F. Izrailev and A. A. Krokhin, *Phys. Rev. Lett.* **82**, 4062 (1999).
3. S. Aubry and G. André, *Ann. Israel Phys. Soc.* **3**, 133 (1980).
4. D. R. Grempell, S. Fishman and R. Prange, *Phys. Rev. Lett.* **49**, 833 (1982).
5. M. Kohmoto, L. P. Kadanoff and C. Tang, *Phys. Rev. Lett.* **50**, 1870 (1983).
6. S. Ostlund *et al.*, *Phys. Rev. Lett.* **50**, 1873 (1983).
7. H. Hiramoto and M. Kohmoto, *Phys. Rev. B* **40**, 8225 (1989).
8. D. J. Boers *et al.*, *Phys. Rev. A* **75**, 063404 (2007).
9. M. Modugno, *New J. Phys.* **11**, 033023 (2009).
10. S. Flach, M. Ivanchenko and R. Khomeriki, *Europhys. Lett.* **98**, 66002 (2012).
11. Y. Lahini *et al.*, *Phys. Rev. Lett.* **103**, 013901 (2009).
12. G. Roati *et al.*, *Nature* **453**, 895 (2008).
13. M. Larcher, F. Dalfovo and M. Mogudno, *Phys. Rev. A* **80**, 053606 (2009).
14. A. Avila and S. Jitomirskaya, *Ann. Math.* **170**, 303 (2009).
15. S. Ya. Jitomirskaya and I. V. Krasovsky, *Math. Res. Lett.* **9**, 413 (2002).
16. A. Avila, arXiv:0810.2965 (2008).
17. S. Ya. Jitomirskaya, *Ann. Math.* **150**, 1159 (1999).
18. A. Gordon *et al.*, *Acta Math.* **178**, 169 (1997).
19. C. Tang and M. Kohmoto, *Phys. Rev. B* **34**, 2041 (1986).
20. J. Bell and R. B. Stinchcombe, *J. Phys. A* **20**, L739 (1987).
21. T. Geisel, R. Ketzmerick and G. Petschel, *Phys. Rev. Lett.* **66**, 1651 (1991).
22. Y. Last, *Commun. Math. Phys.* **164**, 421 (1994).
23. M. Wilkinson and E. J. Austin, *Phys. Rev. B* **50**, 1420 (1994).
24. H. Hiramoto and S. Abe, *J. Phys. Soc. Jpn.* **57**, 1365 (1988).
25. R. Ketzmerick, G. Petschel and T. Geisel, *Phys. Rev. Lett.* **69**, 695 (1992).
26. K. Rayanov, G. Radons and S. Flach, *Phys. Rev. E* **88**, 012901 (2013).
27. N. Levenberg *et al.*, *Proc. Am. Math. Soc.* **104**, 419 (1988).
28. L. Bos and B. Pavlov, Absolute continuity of convolutions of singular measures and new branches of spectrum of Liouvillians and few-body Hamiltonians, in *Generalized Functions, Operator Theory, and Dynamical Systems* (Chapman & Hall CRC, Boca Raton, FL, 1999), pp. 308–322.